ISR WFC3 2025-08

Pixel-Based Non-Linearity Correction for the WFC3 IR Detector

Sachindev S. Shenoy, Ky Huynh, Varun Bajaj, & Jennifer Mack

November 4, 2025

Abstract

The current non-linearity correction for the Wide Field Camera 3 Infrared (WFC3/IR) channel is based on ground-based data acquired during WFC3's Thermal Vacuum 3 (TV3) testing campaign. In the current reference file, the correction coefficients derived for each pixel are averaged over each of the four detector quadrants. In this work, we compute a new pixel-based non-linearity correction using in-flight calibration observations with the internal tungsten lamp flats acquired between 2011 and 2013. We derive the new correction coefficients by fitting a third-order polynomial to the accumulated signal "up-the-ramp" for each pixel. Approximately 2% of IR detector pixels are flagged as bad, and a solution cannot be computed. For these, we use the quadrant averages of the new correction coefficients. An accompanying report (Huynh et al. 2025) provides detailed testing results using both internal flats and external science targets acquired in a variety of observing modes. The report highlights improvements in photometry derived from "_flt.fits" data products calibrated using the new reference file, with the largest improvement for pixels with fluence levels approaching the full well limit of ~80,000 e^-. A new NLINFILE reference file was delivered in October 2025 and will be used to reprocess all WFC3/IR imaging and grism observations in the MAST archive.

Introduction

The Wide Field Camera 3 Infrared (WFC3/IR) channel is a 1024 × 1024 HgCdTe (Mercury Cadmium Telluride) detector built by Teledyne. HgCdTe is one of the most commonly used semiconductor materials to detect IR radiation due to the ability to tune the optical properties of the semiconductor to desired IR wavelengths by choosing the amount of Cd in the alloy (Marinelli and Green 2024). IR radiation detection occurs when a photon impinges on the material, generating electron-hole pairs, where some of the electrons and holes recombine, and the remaining electrons (or holes, depending on the material) are kicked from the valence band to the conduction band. These electrons are then collected by the readout circuit and transformed into an electric signal.

Ideally, as the total number of incident photons increases, the number of electrons in the conduction band increases linearly. However, when the conduction band approaches saturation, the response of the electron deviates from linearity with respect to the incident photons. Due to defects in the material, it has been shown experimentally that the IR detector is inherently non-linear even at low numbers of incident photons.

To correct for the non-linearity effects, we first fit a linear response to low signal levels (reads) to get an "ideal" signal for each pixel, which is then used to normalize the later reads. One can then fit a higher-order polynomial to the normalized signal and record the coefficients of the polynomial fit. These coefficients can then be used to correct the observed science data. The detailed description of this method is provided in the Model Fitting section below. As of 2025, the non-linearity correction coefficients in `calwf3` (WFC3 data processing pipeline) are derived using a similar method but are averaged over an entire quadrant of the detector, hereafter referred to as quad-based correction (Hilbert 2008). In this document, we explore the improvement in the non-linearity correction achieved by deriving the correction coefficients on a per-pixel basis (hereafter referred to as the pixel-based correction), rather than the quad-based correction.

Data Reduction

The standard method to derive the IR non-linearity corrections is to observe flat field data with short and long exposure times, which provides one with both data in the "linear" and "non-linear" regimes, respectively. The WFC3/IR channel uses a MULTIACCUM mode in which the detector signal is read out non-destructively multiple times. There are 12 predefined sample sequences that accommodate a wide range of observing conditions. For this work, we use data from WFC3 in-flight calibration (CAL) programs designed to characterize the non-linearity by obtaining flat-field exposures with the internal tungsten lamps using the SPARS25 sample sequence (Section 7.7.3 - WFC3 Instrument Handbook). This sequence is ideal for characterizing the linearity because it samples (reads out) the detector with a uniform interval of ∼25 seconds. Each flat is read out 15 times, the maximum allowed for the WFC3/IR channel, allowing the majority of detector pixels to become saturated in the last few reads of the exposure. We refer to the set of samples (reads) for an individual exposure as a "ramp" in the rest of this document.

We use a similar dataset that was used in a previous WFC3/IR non-linearity correction study (Hilbert 2014), focusing only on the SPARS25 internal flats. All of the data are part of the non-linearity monitoring WFC3/CAL programs (proposal IDs 12352, 12696, & 13079), which consist of both internal flats and external star cluster data. Internal flats are first acquired in the F126N filter to warm up the lamp and achieve a stable flux. Flats are then acquired in the F127M filter to characterize the non-linearity. Table 1 in Appendix A lists the proposal ID, filter, sample sequence, exposure times, and rootnames of all F127M flat field and dark observations used. Internal flats from the first non-linearity CAL program, 11931, did not allow for sufficient lamp warm-up time and were therefore excluded from both studies.

Previous calibration observations (K. S. Long, Wheeler, and Bushouse 2011; K. S. Long and Baggett 2018) have shown that WFC3/IR suffers from persistence issues, and one needs to plan for persistence mitigation during observations (Knox S. Long et al. 2010). Dark frames are obtained before and after the flat observations to monitor persistence. This was fortuitous, allowing us to use the zeroth read (the detector readout at 2.932 sec after the start of the dark observation) as the bias level in our data reduction. In the normal WFC3/IR data reduction pipeline, `calwf3`, the reference pixels located at the periphery of the detector are used to compute a σ-clipped mean signal, which is used as a bias level. While this is a good estimation of the detector bias level, it does not represent the pixel-to-pixel variations in the bias signal, which we must account for when deriving a pixel-based non-linearity correction. We thus elected to use the zeroth read of the dark observations as the bias, rather than the σ-clipped mean calculated from the reference pixels.

In addition to the lamp flats, these WFC3/CAL programs also included external observations of the star cluster 47 Tucanae, consisting of both short and long exposures in the F160W filter. These observations were designed to test the non-linearity solution derived from lamp flats and are discussed in an accompanying report (Huynh et al. 2025), which compares photometry derived with the new pixel-based non-linearity correction with the current quad-based correction.

The general procedure for deriving the non-linearity correction coefficients is listed below, and the details are described in the following sections:

- Download the data (RAW, and IMA data products) from the MAST archive. A total of 23 F127M flat field exposures and 23 corresponding dark frames from the three aforementioned CAL programs were used to derive the pixel-based non-linearity correction (see Table 1).

- Group the data into individual visits, which include the RAW and IMA data products for the internal flat and the corresponding dark.

- Examine the IMA data products to identify pixels flagged in the DQ array and to estimate the percentage of detector pixels that may fail during the fitting step. Pixels with a DQ flag value = 8192, corresponding to cosmic ray (CR) hits, were specifically inspected. These can produce discontinuities or jumps in the ramp signal, which can adversely affect the fitting process.

- Perform a bias subtraction using the zeroth read of the preceding dark observation as a bias frame.
- Mean combine each of the ramps for all the flat observations to generate a master flat.
- Flag all pixels that are either dead, saturated in early reads, or hard saturated (defined as pixels exceeding 25% non-linearity).
- Fit a linear model to the first three reads to estimate an ideal response. For more details, see the Model Fitting section, Equation 1, and Figure 3.
- Normalize the master flat with the ideal response to derive a fractional linearity.
- Fit a polynomial equation to the fractional linearity to derive the non-linearity correction coefficients.
- For bad pixels, which are masked and have a NaN value, use the quadrant-based averages of the new coefficients as the correction coefficients.
- Generate the non-linearity correction reference file with an appropriate format that can be used with the WFC3 data reduction pipeline, `calwf3`. For details on the file format, see Table 2.

Data Cleaning

All of the RAW and calibrated IMA files for both the internal flat observations and their associated darks were downloaded using the `astroquery` Application Programming Interface (API). Inspection of the DQ flags in the IMA files showed that, on average, 1.95 ± 0.01 % of the pixels in a given read are flagged for various reasons such as dead pixels (DQ=4), hot pixels (DQ=16), or unstable pixels (DQ=32). See Table 2.7 in Section 2.2.3 in Pagul and Rivera 2024 for a complete list of DQ flags. Given the large number of input observations available for generating the master flat, we possess sufficient statistics to detect and exclude outliers (bad pixels) during the merging process. We therefore did not flag any bad pixels at this stage; however, we did investigate those pixels identified as cosmic ray hits.

Cosmic ray (CR) impacts are flagged in the IMA file (DQ=8192) during the "up-the-ramp" fitting step in `calwf3`, which looks for jumps in the rate signal that deviates by more than 4-sigma from the expected linear response (see Section 3.3.10 of the WFC3 Data Handbook, Pagul and Rivera 2024). We find that SPARS25 flats calibrated using the 2008 quadrant-based reference file have overly aggressive CR flagging, setting the DQ flag for a large fraction of detector pixels. Once a CR flag is set in a given read of the IMA file, all subsequent reads for that pixel are flagged. Furthermore, the majority of these pixels had additional DQ flags set, complicating the isolation of pure CR impacts. This issue precludes masking pixels flagged as CR hits, as this would exclude a substantial number ($\approx 30\%$) of pixels from the linearity fitting. Further investigation into the pipeline's CR flagging settings and the appropriate rejection threshold for different IR sample sequences is beyond the scope of this document.

Bias subtraction

The WFC3/IR channel exhibits a bias signal arising from the DC offset applied to the detector, fixed pattern noise, and readout noise. A nominal step in IR data processing is to subtract a bias frame from each input data frame. For WFC3/IR, we must subtract this bias signal from each of the ramp reads. Therefore, a dedicated bias observation concurrent with the flat observation is essential for obtaining an accurately bias-subtracted flat. Since all calibration programs included a dark frame before and after the flat observations, we utilized the zeroth read of the preceding dark frame as our bias signal. We did not use the zeroth read of the flat observation as a bias signal, despite it having the same readout time ($\sim 3\ s$) as the dark, because it includes additional signal from the internal lamp. Although a master bias generated from all dark observations would increase the signal-to-noise ratio, its noise profile is sufficiently different from that of the individual flat, which would introduce a non-optimal noise profile during subtraction.

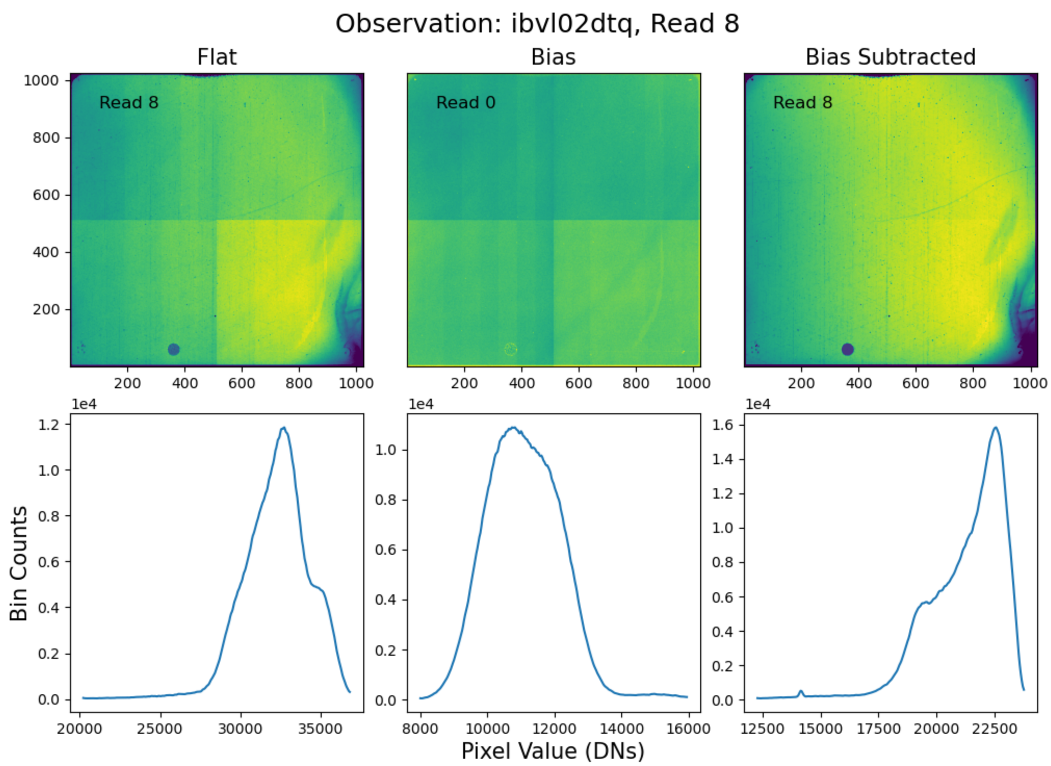

Figure 1: Example of bias-subtracted data. The first column shows the flat SCI array, the middle column is the bias frame (zeroth read of a RAW dark file), and the last column is the bias-subtracted flat. The second row is a histogram of pixel values for each respective frame. Images in the top row are displayed in a linear scale with zscale interval.

Figure 1 shows an example of bias subtraction, where the left panel shows read 8 of the RAW flat data, the middle panel shows read 0 of the dark data used as a bias signal, and the right panel shows read 8 of the bias-subtracted data. Analysis of the bias-subtracted flats showed that overall, this process produced a nominal flat. However, in each of the individual observations, a small subset of pixels had very low pixel values, resulting either from a non-responsive pixel in the flat or an abnormally high value in the bias. These pixels would get flagged by the outlier rejection when generating the master flat, but will need additional scrutiny during the fitting process.

Generate Master Flat

Ideally, one can fit a polynomial model to the individual bias-subtracted flat, but due to the higher noise in the individual observations, the fits are not well constrained, which results in derived correction coefficients with higher uncertainties. Assuming that the read noise and non-linear response do not vary from image to image, we combine the bias-subtracted flats to generate a master flat before fitting a polynomial model. Each of the ramps in the bias-subtracted flats were combined using a 3-σ clipped mean with associated uncertainties propagated. In the previous steps, we have not masked any bad pixels, as the outlier rejection will exclude most of these bad pixels. However, inspection of the master flat showed that three kinds of pixel responses needed to be flagged and excluded from the fitting. These three non-optimal responses are:

Early saturated pixels: Pixels that reach the maximum fluence level (saturation) within the first two reads. In the master flat, we detected about 100 pixels that reached maximum fluence values in the first read and about 50 pixels in the second read. Since the saturation was reached in the early reads, we flagged all the reads on this set and excluded them from fitting.

Dead pixels: Pixels whose fluence values were always below 100 counts for all the reads. We found about a dozen pixels that showed this behavior.

Hard saturated pixels: Pixels that reached the well depth limit before the end of the entire ramp sequence. Since not all of the pixels in a given detector are uniform, they tend to reach their well depth at different fluence levels. We detected these pixels by fitting a linear response to the first three reads and then estimating the percent difference for each pixel up the ramp. We flagged any pixel that was 25% lower than the linear model to indicate that these pixels were reaching their well depth limits. For most of the non-linearity coefficient calculations in the IR detector, it is nominal to set a pixel as saturated when it is 5% lower than the linear model. So our limit of 25% is well beyond this nominal value and will probe the highly non-linear regime as the pixel approaches the well depth limit.

We save the indices of these flagged pixels to be used later in the reduction process. Figure 2 (top panels) shows the SCI and ERR arrays of the last read of the master flat file, along with the location of flagged pixels. The bottom panel in the figure shows a histogram of the pixel value (DN) in the SCI and ERR arrays, respectively.

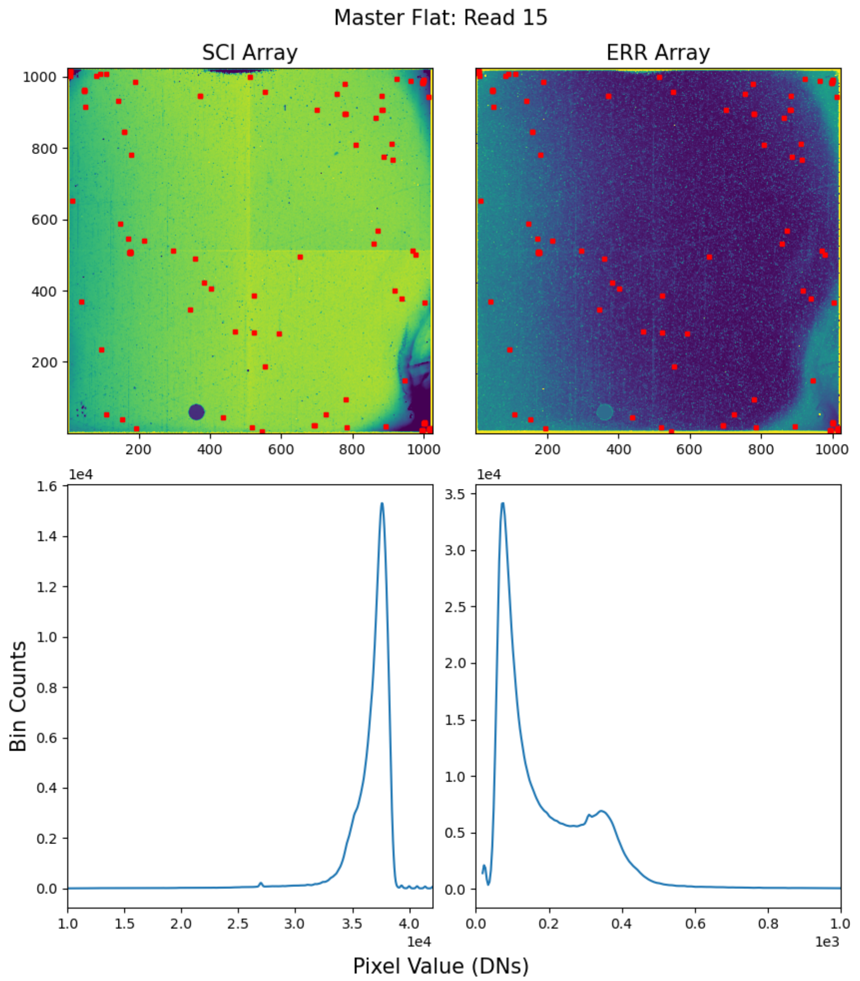

Figure 2: The top row displays the cumulative read of the SCI and ERR arrays from the master flat. The red squares are early saturated pixels, dead pixels, and hard saturated pixels. The bottom row is the histogram of pixel values in the SCI and ERR arrays, respectively. The images in the top row are displayed in a linear scale with zscale interval.

Model Fitting

After merging and cleaning the data, we start the determination of the non-linear coefficients by fitting an ideal response (see Figure 3) and using it to calculate the fractional linearity. Since we already fit a linear function to early reads of the ramp in order to flag pixels that reach their well depth limit (see the "Generate Master Flat" section), we can use the same fit results to get an ideal signal across all reads and use it to determine fractional linearity. The "ideal" signal is given by:

$$y_{ij\ ideal} = m_{ij} * t_{ij} + c_{ij} \tag{1}$$

where $y_{ij\ ideal}$ is the measured signal for pixel index (i, j) at time t, m_{ij} and c_{ij} are the slope and intercept of the linear model, respectively.

Note that the use of this ideal response equation relies on two primary assumptions.

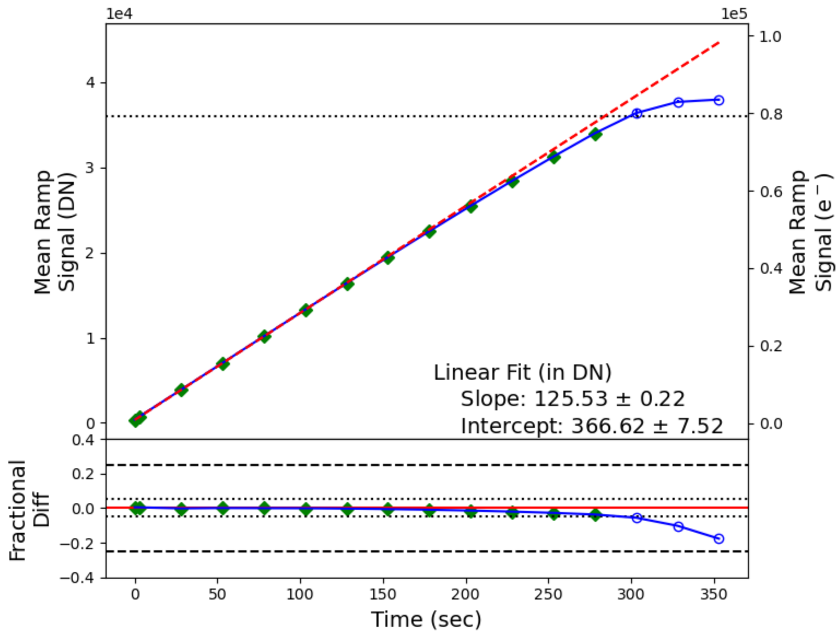

Figure 3: WFC3/IR non-linear response of the mean signal (DN) in the master flat as a function of sample time (sec). Top Panel: Shows the mean signal in the master flat for a sample pixel (indices 465, 987). The green diamonds represent the mean signal values. The red dashed line is the linear fit derived from the first four reads. The horizontal black dotted line indicates the pixel's saturation limit. Blue open circles highlight mean signal values exceeding this saturation limit. Bottom Panel: Displays the fractional difference between the mean signal and the linear fit shown in the top panel. The dotted and dashed lines indicate the 5% and 25% difference thresholds, respectively.

The first assumption is that the first three (or more) reads exhibit a linear response, a premise that is often invalid. Previous studies (Robberto 2010; Robberto 2011) have suggested that no fluence regime shows purely linear pixel response, with non-linear behavior occurring even at the lowest fluence levels. Recently, test using data from SPARS10 flats show that non-linearity effects at low fluence levels are on the order of 1% (see Huynh et al. 2025, Figure 4). However, due to the sparse sampling sequence of SPARS25 at low fluence levels, we are unable to determine the higher-order coefficients and must, therefore, assume a linear response in this region.

We investigated the possibility of merging our data with flat observations taken using a different sample sequence with shorter read intervals. This, in principle, will yield additional data points in the low fluence region and will help in determining higher-order terms in the polynomial fit. Though, we found that the merged dataset resulted in an offset between data from the two sample sequences. Since the bias levels for each pixel is different between the two sample sequences, merging the datasets is not trivial. As such, we chose to use only the one sample sequence (SPARS25) and maintain the assumption of a linear response in the low fluence region. To further explore these issues we plan to get additional calibration observations using SPARS5 flats that will be acquired in Cycle 33 (program 17957).

Our second assumption involves the use of an intercept term ($c_{i,j}$), despite the input data being bias-subtracted. This is essential because the bias subtraction is imperfect, and the intercept accounts for any residual offset. Allowing a non-zero intercept ensures that even pixels affected by large errors in the bias subtraction will yield reasonably accurate fit coefficients.

Figure 3 shows an example of the non-linear response for a pixel with indices (465, 987) in the master flat. The plot shows the mean ramp signal (in DN) as a function of time in the top panel and the fractional difference between the measured data and the linear fit in the bottom panel. The diamond data points in the top panel are the measured signal, the red dashed line is the linear fit to the first four reads (roughly for signal up to 10,000 DN), and the black dotted line is the saturation limit for this pixel where the measured signal deviates more than 5% from the linear fit. In both panels, the green diamonds and blue open circles refer to data that is below and above the saturation limit (percent difference < 5%), respectively. (A map of the full well limit is provided in Figure 6 of Appendix C and highlights both pixel-to-pixel and spatial variations across the detector.)

Next, we define the fractional linearity (Equation 2) as normalizing the observed signal by the ideal signal, which is identical to the factional difference data shown in the bottom panel of Figure 3. As seen in the figure, this residual signal will now consist of only the non-linear terms and can be used to fit a higher-order polynomial.

$$F_{ij\ Lin} = \frac{y_{ij\ obs}}{y_{ij\ ideal}} \tag{2}$$

Lastly, we use a third-order polynomial to fit the fractional linearity and derive the non-linearity correction coefficients, as shown in Equation 3).

$$F_{ij\ Lin} = 1 - (\alpha_{ij} + \beta_{ij} * y_{ij\ obs} + \gamma_{ij} * y^2_{ij\ obs} + \delta_{ij} * y^3_{ij\ obs}) \tag{3}$$

where α_{ij}, β_{ij}, γ_{ij}, and δ_{ij} are the fit coefficients and $y_{ij\ obs}$ is the observed signal in the ramp. These derived coefficients are then used to correct the observed signal, a process implemented in the `NLINCORR` step of `calwf3` (§ 3.3.7 in Pagul and Rivera 2024).

We now have a set of coefficients that correct the non-linear response for most pixels, with two exceptions:

- Non-nominal pixels that were masked after the master flat derivation.
- Pixels where the curve fitting failed.

Fitting failure can occur for various reasons, such as a lack of available reads (due to later reads saturating) or fits that converged to a local, rather than a global, minimum. For both cases, we replace their coefficients with a 3-σ clipped median of the correction coefficients in their individual detector quadrants.

Finally, the data is reformatted to ensure compatibility with `calwf3` execution. The structure of the flat reference file is described in Appendix B. For technical details on the detector non-linearity correction applied during the `NLINCORR` step, refer to the `calwf3` documentation.

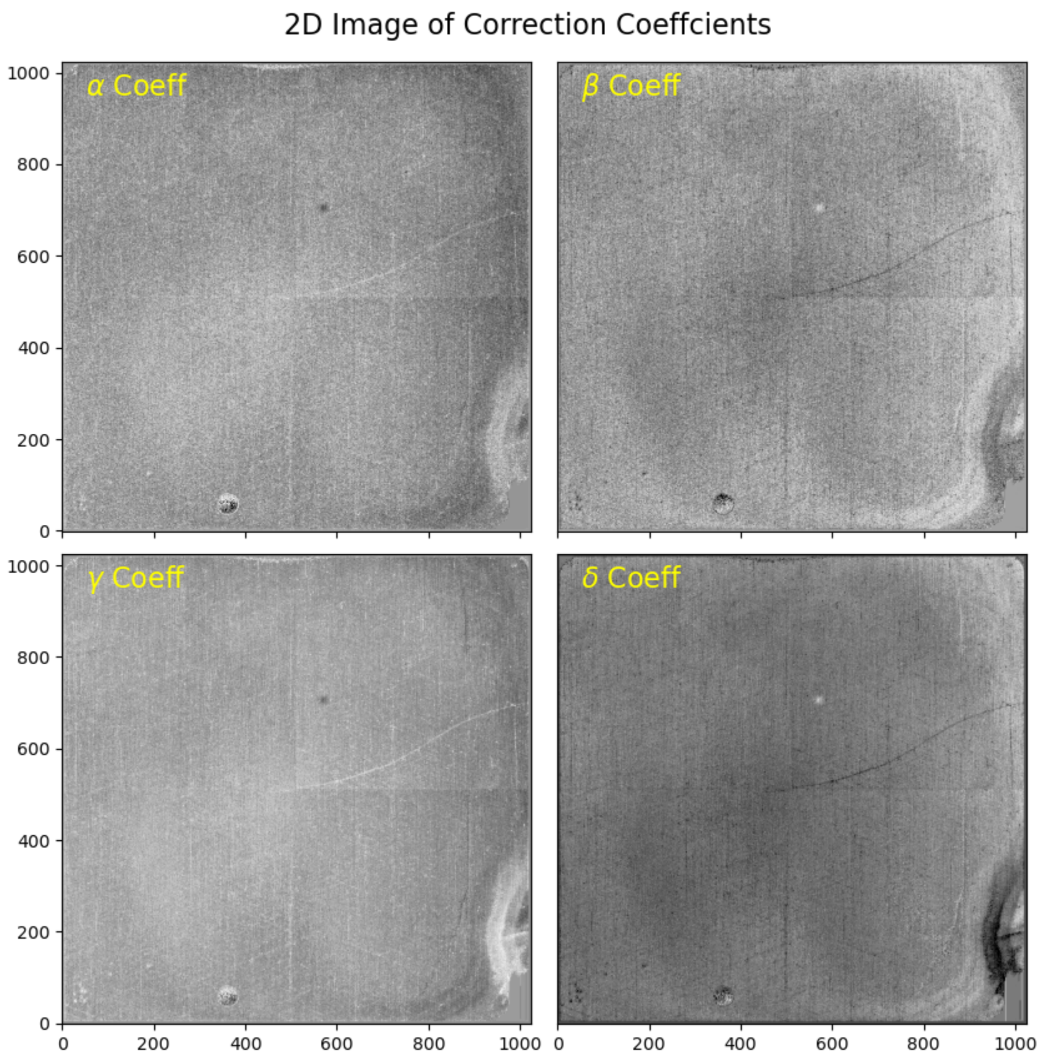

Figure 4: Maps of the four fit coefficients derived using the model in Equation 3. The coefficients are labeled at the top of each image and highlight both pixel-to-pixel and large-scale variations across the detector. In each image, the data is displayed with a linear scale and zscale interval.

Figure 4 displays the four non-linearity correction coefficients from the pixel-based reference file. Because these coefficients were derived for individual pixels of the WFC3/IR detector, they exhibit the same detector artifacts observed in the raw and processed data (e.g., the wagon wheel, death star, and un-bonded pixels). Figure 5 shows histogram plots of these four coefficients. A notable feature in these plots is the spikes (high bin counts)

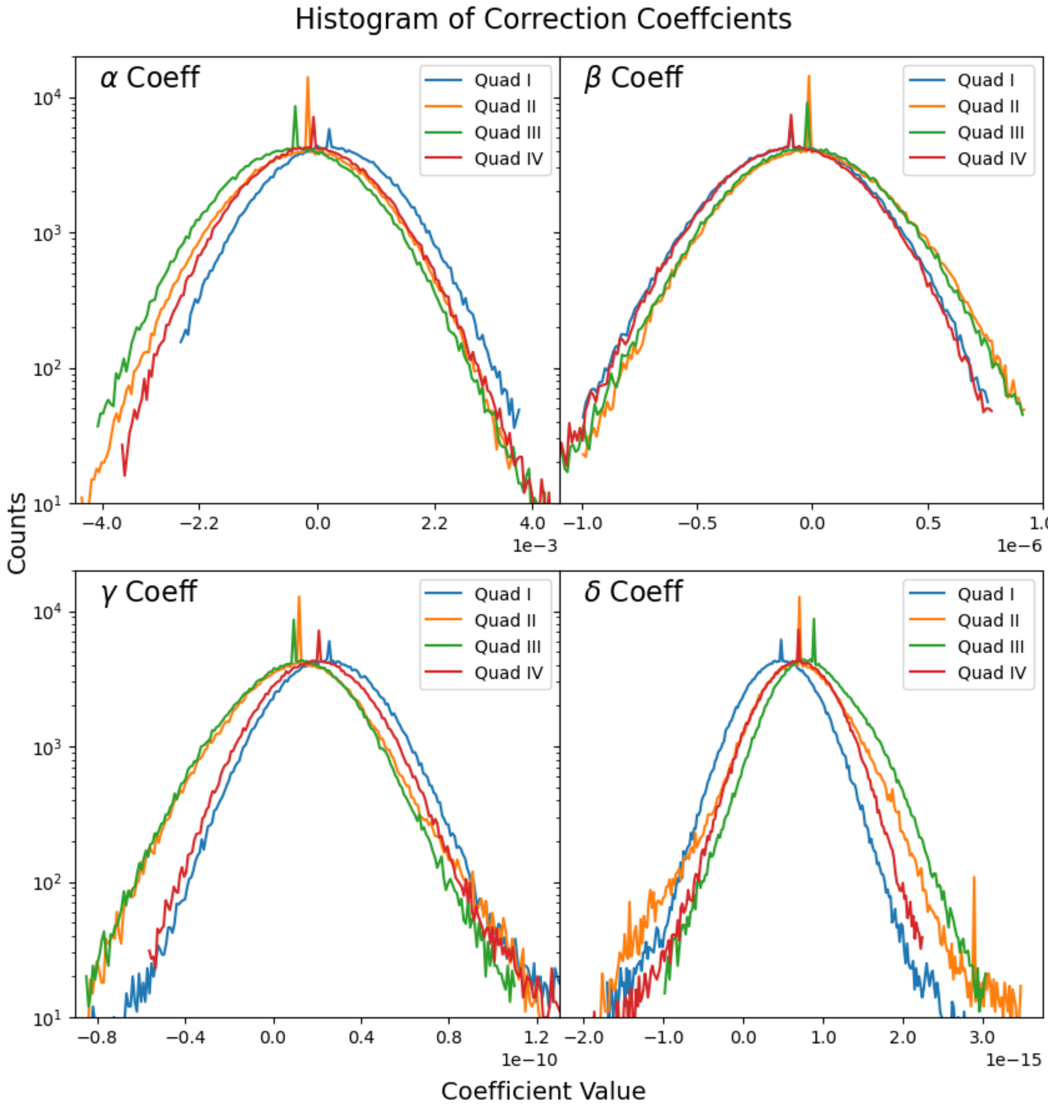

Figure 5: Histogram of the four non-linearity correction coefficient values derived for each quadrant of the WFC3 IR detector using the model in Equation 3.The four coefficients are labeled in the top-left of each plot, and the quadrant IDs are labeled in the top-right box. The spikes observed at the peak of each histogram originate from bad pixels where the NaN values have been replaced with a quadrant-based average of the correction coefficients.

overlaid on the peak of the histogram. These spikes result from replacing the NaN values for masked and poor-fit pixels with the quadrant-based averages of the correction coefficients, as described previously.

Analysis

Detailed testing of the new pixel-based, non-linearity correction file is described in an accompanying report WFC3 ISR 2025-09 by Huynh et al. (2025), available from the WFC3 Instrument Science Reports page.

Testing was performed for a variety of targets and observing modes, including: internal flat fields, star clusters, and HST flux standards (imaging and grism data) acquired in a wide range of sample sequences. In general, the new correction improves the linearity for sources with fluence levels above ∼50,000 e^- (∼20,000 DN), with improvements up to 7% for pixels with fluence levels approaching the saturation limit of ∼80,000 e^- in the last unsaturated reads of the IMA file. The effect is smaller in FLT data products, with improvements of up to ∼0.5% in a 3-pixel aperture radius. The pixel-based solution also significantly decreases the number of cosmic rays flagged during `calwf3`'s up-the-ramp fit, leading to improved photometric accuracy and higher signal-to-noise in the calibrated FLT data products.

The new correction has a negligible impact (∼0.1–0.2%) on the published IR zeropoints by Calamida et al. (2024) and will therefore be implemented in the `calwf3` pipeline without updating the WFC3/IR image photometry reference file (IMPHTTAB). For additional details, see the "IR Zeropoints" section of WFC3 ISR 2025-09 by Huynh et al. (2025).

Caveats

Whilst this analysis yields a new non-linearity solution with significant improvement in the high-fluence regime, a number of caveats may still persist, and could be improved upon in future work.

First, the limited number of samples obtainable in a single WFC3/IR exposure (15) limits the overall precision of the non-linearity calibration. As a pixel approaches saturation, the non-linearity of the pixel's response to incident photons increases. If a pixel reaches saturation between read_i and read_{i+1}, the signal measured at read_{i+1} cannot be used to quantify the non-linear response. Thus, to measure the pixel's response right up to the saturation limit, a read must occur just before the signal reaches the saturation limit. With full-well depths in the range of 70,000 - 80,000 e^-, and only 15 samples (which can only occur evenly spaced at the end of the ramp), this is unlikely. Thus, the high-fluence regime will have higher uncertainties than the mid-fluence regime.

In addition, the relation between cosmic ray flagging and non-linearity is somewhat circular, as the cosmic ray flagging algorithm assumes the signal in a pixel accumulates linearly over the course of the ramp. However, if the signal is non-linear (even after applying the linearity calibration), any deviation from linearity can result in pixels being flagged in error as cosmic rays, even if the pixel did not receive a real cosmic ray impact. As the creation of the non-linearity reference file requires cosmic rays to be masked (real jump discontinuities in the signal would invalidate the polynomial fits), cosmic ray hit pixels are removed before the creation of the master flat. As a result, some of the most non-linear pixels may be systematically removed from this analysis (and thus not fully calibrated) due to erroneous cosmic ray flagging. To fix this, an iterative approach would need to be applied, solving for the linearity coefficients and incrementally increasing the cosmic ray detection sensitivity repeatedly until a convergent solution is found.

Lastly, the non-linearity in the low fluence regime adds further uncertainty to this calibration. As this analysis assumes the first few reads are linear (with a potential nonzero intercept), the y_{ideal} signal used to normalize y_{obs} introduces a small error to the correction in the low fluence end (1-2%), where the correction is typically dominated by the linear term of the solution. As the first few reads of the SPARS25 internal flats span the first 10-20% of the full well depth, this error may affect the calibration for pixels imaging fainter sources. In theory, leveraging data taken using other sample sequences may allow for finer sampling in the low-fluence regime and allow for a reduction in this error. However, combining data from the various sample sequences requires more careful consideration and is out of the scope of this document.

Summary

We outline the methodology for creating a new pixel-based non-linearity correction for the WFC3/IR detector, which improves upon the current quadrant-based correction derived from ground test data. Utilizing SPARS25 internal flats acquired on-orbit over 3 years of CAL/WFC3 non-linearity monitoring programs, we generate a bias-subtracted master flat.

Using this master flat, we derive linearity correction coefficients for each pixel modeled by a third-order polynomial. We are unable to derive correction coefficients for ∼2% of detector pixels which are known to be bad. For these, we replaced their values with quadrant-based averages calculated from the newly derived corrections.

Testing by Huynh et al. (2025) shows that the current quadrant-based correction and the new pixel-based correction perform similarly for low fluence levels (<50,000 e^-). However, at higher fluence levels (∼50,000 - 80,000 e^-), the pixel-based correction improves the linearity by up to 7% in the last reads of the IMA file just before saturation. The effect is smaller in FLT images after the ramp fit in `calwf3`, with improvements of up to ∼0.5% in the observed photometry of bright stars in a 3-pixel aperture radius.

The updated non-linearity reference file `9au15283i_lin.fits` was delivered to the Calibration Database Reference System in October 2025 and will be used to reprocess all WFC3/IR imaging and grism observations in the MAST archive by late-2025.

Acknowledgements

We appreciate the careful review of this work by Benjamin Kuhn, Joel Green, Norman Grogin, & Sylvia Baggett and would like to thank them for their suggestions to improve the quality of this report. We would also like to thank the WFC3 Photometry team and Peter

McCullough for help in critiquing this work and their helpful suggestions in improving this project.

References

Calamida, Annalisa et al. (Dec. 2024). *New Time-Dependent WFC3/IR Inverse Sensitivities*. Instrument Science Report WFC3 2024-13, 22 pages.

Hilbert, B. (Jan. 2008). *WFC3 TV3 Testing: IR Channel Nonlinearity Correction*. Instrument Science Report WFC3 2008-39, 14 pages.

— (July 2014). *Updated non-linearity calibration method for WFC3/IR*. WFC3 Instrument Science Report 2014-17.

Huynh, K. et al. (Sept. 2025). *Testing and Validation of the Updated Pixel-Based Non-Linearity Calibration File for WFC3/IR*. WFC3 Instrument Science Report 2025-09.

Long, K. S. and S. M. Baggett (Mar. 2018). *Persistence in the WFC3 IR Detector: Intrinsic Variability*. WFC3 Instrument Science Report 2018-03.

Long, K. S., T. Wheeler, and H. Bushouse (Apr. 2011). *IR Detector Timing and Persistence*. WFC3 Instrument Science Report 2011-09.

Long, Knox S. et al. (Nov. 2010). *WFC3/IR Persistence as Measured in Cycle 17 using Tungsten Lamp Exposures*. WFC3 Instrument Science Report 2010-17, 12 pages.

Marinelli, Mariarosa and Joel Green (2024). "WFC3 Instrument Handbook for Cycle 33 v. 17.0". In: *WFC3 Instrument Handbook for Cycle 33 v. 17*. Vol. 17, p. 17.

Pagul, Amanda and Isabel Rivera (2024). "WFC3 Data Handbook v. 6". In: *WFC3 Data Handbook v. 6*. Vol. 6, p. 6.

Robberto, M. (July 2010). *An improved algorithm for the correction of IR detector non-linearity*. JWST-STScI-CR-002163.

— (Jan. 2011). *Implimentation of a new algorithm for the correction of non-linearity in JWST detectors*. JWST-STScI-CR-002346.

Appendix A Input Manifest

The table below lists the input data that was used to generate the master flat used in deriving the non-linearity correction coefficients. All of the data was collected as part of three WFC3/IR Linearity Monitoring programs. The table only includes the identities of flats in F127M and dark observations; all of the other observations in each program are excluded from this work. Observations were taken from March 2011 to April 2013.

Table 1: Flat field & dark current exposures used to derive the non-linearity coefficients for the WFC3/IR detector.

Proposal ID	Filter	Sample Sequence	Exposure Time (sec)	Observation ID
12352	Blank	SPARS25, NSAMP=12	252.9	ibmg02sfq, ibmg03a7q, ibmg04ceq, ibmg05dcq, ibmg06eaq, ibmg07jkq, ibmg10uvq, ibmg13gsq, ibmg14q3q, ibmg15qnq, ibmg16r9q
12352	F127M	SPARS25, NSAMP=16	352.9	ibmg02siq, ibmg03aaq, ibmg04chq, ibmg07jtq, ibmg05dfq, ibmg06edq, ibmg14q6q, ibmg10uzq, ibmg13gvq, ibmg15qqq, ibmg16rcq
12696	Blank	SPARS25, NSAMP=12	252.9	ibvl01adq, ibvl02dqq, ibvl03f2q, ibvl04kbq, ibvl05o8q, ibvl13soq, ibvl14ovq, ibvl15fxq, ibvl16k2q
12696	F127M	SPARS25, NSAMP=16	352.9	ibvl01ahq, ibvl02dtq, ibvl03f5q, ibvl04khq, ibvl05obq, ibvl13suq, ibvl14p2q, ibvl15g0q, ibvl16k6q
13079	Blank	SPARS25, NSAMP=12	252.9	ic5n07jlq, ic5n08khq, ic5n09mwq
13079	F127M	SPARS25, NSAMP=16	352.9	ic5n07joq, ic5n08kkq, ic5n09mzq

Appendix B Reference File Data Format

The non-linearity correction reference file, as described in §11.2.8 of HST Reference Files Information Document, is stored in a standard FITS format with multiple COEF and ERR extensions and a single DQ, NODE, ZSCI, & ZERR extensions with the same dimensions as the WFC3 IR detector array (1024x1024).

The correction coefficients are stored in floating-point image extensions with EXTNAME set to COEF and EXTVER ranging from 1 to 4, denoting the 4 coefficients from Equation 3.

The polynomial model (Equation 3) fit variance of these coefficients are stored in the image extension with EXTNAME set to ERR and EXTVER ranging from 1 to 4, while the covariance terms are saved with EXTNAME set to ERR and EXTVER ranging from 5 to 10.

Table 2: Linearity correction reference file data format.

Ext. No.	EXTNAME	EXTVER	BITPIX	Dimension	Description
0	N/A	N/A	8	N/A	Primary header (no data)
1	COEF	1	-32	1024x1024	Linearity coefficient α
2	COEF	2	-32	1024x1024	Linearity β
3	COEF	3	-32	1024x1024	Linearity γ
4	COEF	4	-32	1024x1024	Linearity δ
5	ERR	1	-32	1024x1024	Variance α
6	ERR	2	-32	1024x1024	Variance β
7	ERR	3	-32	1024x1024	Variance γ
8	ERR	4	-32	1024x1024	Variance δ
9	ERR	5	-32	1024x1024	Covariance $\alpha\beta$
10	ERR	6	-32	1024x1024	Covariance $\beta\gamma$
11	ERR	7	-32	1024x1024	Covariance $\gamma\delta$
12	ERR	8	-32	1024x1024	Covariance $\alpha\gamma$
13	ERR	9	-32	1024x1024	Covariance $\beta\delta$
14	ERR	10	-32	1024x1024	Covariance $\alpha\delta$
15	DQ	1	16	1024x1024	Data quality flags
16	NODE	1	-64	1024x1024	Saturation threshold
17	ZSCI	1	-32	1024x1024	Super zero read
18	ZERR	1	-32	1024x1024	Uncertainties in zero read

The data quality flags are stored in [DQ, 1] extension of the FITS file. The saturation map, which defines the full well limit for each individual pixel, is contained in the NODE extension of the FITS file. Figure 6 displays the map in units of DN and is unchanged from the analysis by (Hilbert 2008) using saturated STEP50 flats acquired during ground testing. (The pixel values in this extension are identical in the quad-based and in the pixel-based NLINFILE).

The last two extensions of the non-linearity correction reference file contains the super zero read and its statistical error images with EXTNAME ZSCI & ZERR and EXTVER set to 1. For ease of comprehension, the structure of the non-linearity correction reference file is also shown in a table format in Table 2.

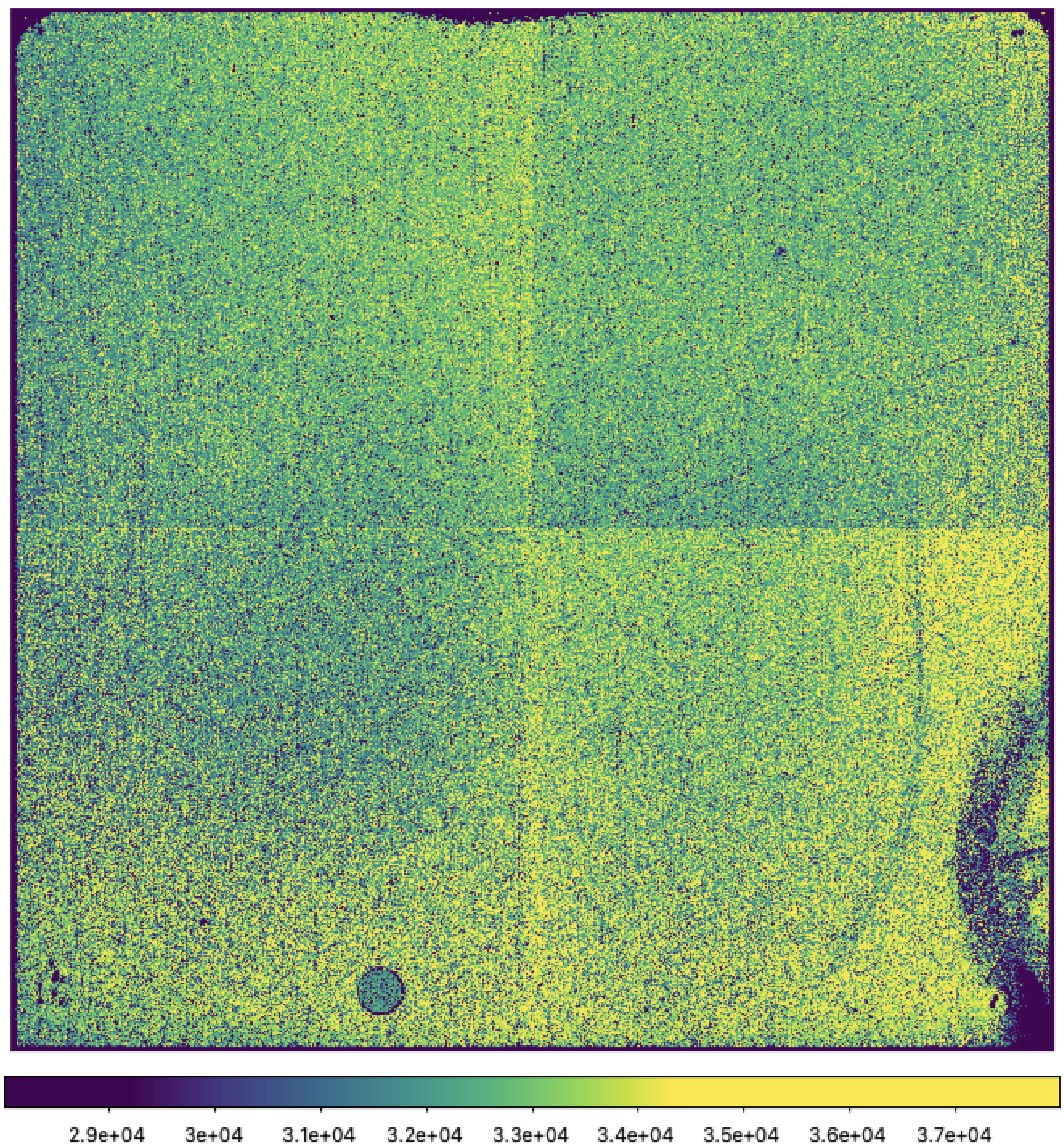

Figure 6: Saturation map defining the full well limit for every pixel on the WFC3/IR channel. The color bar is in units of DN. The saturation map is populated in the NODE extension (EXT = 16) of the NLINFILE. The values in this extension are unchanged from the original analysis by (Hilbert 2008).